# High-$T_c$ Superconducting Fourth-Harmonic Mixer using a Dual-Band Terahertz On-Chip Antenna of High Coupling Efficiency

Xiang Gao, Jia Du, Ting Zhang, and Y. Jay Guo, *Fellow, IEEE*

***Abstract*—This paper presents a dual-band on-chip antenna coupled high-$T_c$ superconducting (HTS) Josephson-junction sub-terahertz (THz) fourth-harmonic mixer. The antenna utilizes a couple of different structured twin-slots to enable the resonant radiations at two frequencies, and integrates a well-designed coplanar waveguide (CPW) network for achieving good radiation coupling and signal isolation characteristics. The electromagnetic (EM) simulations show that coupling efficiencies as high as -4 dB and -3.5 dB are achieved for the 160-GHz and 640-GHz operating frequency bands, respectively. Based on this dual-band antenna, a 640-GHz HTS fourth-harmonic mixer is developed and characterized in a range of operating temperatures. The mixer exhibits a measured conversion gain of around -18 dB at 20 K and -22 dB at 40 K respectively. The achieved intermediate-frequency (IF) bandwidth is larger than 23 GHz. These are the best results reported for HTS harmonic mixers at comparable sub-THz frequency bands to date.**

***Index Terms*—Terahertz mixer, high-temperature superconductor Josephson junction, dual-band on-chip antenna, fourth-harmonic mixing, terahertz wireless applications.**

## I. Introduction

Terahertz (THz) communication [1], [2] and sensing [3] are vitally important wireless technologies that have attracted rapidly growing interest among worldwide researchers in recent years. The abundant bandwidth resource enables low-THz-band (0.1-1 THz) communication to be a potential solution to the issues of data rate and capacity limitations in current wireless systems. The shorter wavelength of sub-THz wave compared with that of microwave and millimeter waves, is beneficial to achieving high spatial resolution whilst maintaining the system compact and lightweight for remote sensing applications. Nevertheless, due to the limited transmitting power and severe atmospheric attenuation at the sub-THz frequencies, an ultrasensitive heterodyne receiver is very much desired for effective signal detection.

Semiconductor-based heterodyne receivers have been widely exploited using Schottky barrier diodes (SBDs) [4], high-electron-mobility transistors (HEMTs) [5], complementary metal-oxide-semiconductor (CMOS) [6] and SiGe [7] technologies. They offer an advantage of being able to operate at room temperature (RT), but requires a relatively high local oscillator (LO) power that poses the challenge as the operating frequency rises. Low-$T_c$ superconducting (LTS) hot electron bolometer (HEB) mixers [8] and superconductor-insulator-superconductor (SIS) mixers [9] operate under much lower LO power and serve as the most sensitive frequency down-converters to date. However, those LTS devices need to be cooled to liquid helium temperature (4.3 K) or below requiring bulky and expensive cryogenic facilities and thus are primarily limited to application in astronomical observation. For sub-THz wireless communication and sensing systems, high-$T_c$ superconducting (HTS) Josephson-junction mixers are promising candidates for receiver frontends considering their combined advantages of superior sensitivity, large bandwidth, low LO power, and lower cryogenic cost (compared to that for cooling the low-$T_c$ superconducting counterparts).

Current research progress on HTS THz or sub-THz mixers is still in its infancy. Early demonstrations were mostly achieved in the temperature ranges below 20 K [10]-[13] and later at 58 K [14]. Recently, HTS Josephson sub-THz mixers that operate up to 77 K have been demonstrated at CSIRO laboratory [15]-[18] using a step-edge junction technology [19]. These reported HTS devices can be divided into fundamental and high-order harmonic mixers according to their operating modes. The former typically exhibit higher mixer conversion gains but require expensive sub-THz sources to offer LO pumping at similar frequencies as that of the received signals. In comparison, the latter utilize microwave LO sources instead thus reducing the costs of the systems. However, they suffer from considerable performance degradation associated with large harmonic numbers. The disadvantages for both operating modes become more serious for higher frequencies (e.g. above 600 GHz). In this case, low-order harmonic mixing makes very good compromise between the cost and performance for the sub-THz receiver systems.

To exploit the potential of HTS mixers, high-performance on-chip antennas are required to effectively couple the sub-THz radiations into the Josephson junctions. Typical thin-film antennas based on the planar log-periodic [11] or spiral [14]

X. Gao and J. Du are with the Commonwealth Scientific and Industrial Research Organization (CSIRO) Manufacturing, Lindfield, NSW 2070, Australia. (e-mail: Xiang.Gao@csiro.au, Jia.Du@csiro.au).

T. Zhang and Y. J. Guo are with the Global Big Data Technologies Centre, University of Technology Sydney, Ultimo, NSW 2007, Australia. (e-mail: Ting.Zhang@uts.edu.au, Jay.Guo@uts.edu.au).

structures, exhibit stable radiation characteristics over a very wide available bandwidth. However, such complementary radiators [20] generally feature an input impedance of around 80 Ω, which is significantly higher than the Josephson junction normal resistance of only a few Ω. This results in a poor coupling efficiency when applied for the HTS Josephson-junction mixers. Other reported on-chip antennas like ring-slot [15] and twin-slot [21] radiators are much more efficient in coupling the radiation, but they are limited to narrowband operation only and not suitable for wideband or multiband applications.

In this paper, we present our latest result of a dual-band on-chip antenna coupled HTS Josephson fourth-harmonic mixer. Two major innovative contributions in this work are highlighted here. (1) A dual-band on-chip antenna was proposed and designed for HTS sub-THz mixers. The antenna's operation principle was clarified through the surface electric current distribution, and detailed simulation analyses were performed to achieve high coupling efficiency and good radiation performance at two frequencies. This is the first reported on-chip antenna that can efficiently couple the radiation into the Josephson junction at multiple frequency bands. (2) A 640-GHz HTS Josephson-junction fourth-harmonic mixer was developed using the dual-band on-chip antenna. The mixer prototype was fabricated, fully packaged and experimentally characterized in a cryocooler [22]. This is the first demonstration of low-order HTS harmonic mixing at such high frequencies (above 600 GHz). Detailed measurement results have shown that the best device performance has been achieved compared to the HTS harmonic mixers reported to date.

## II. Dual-Band Sub-THz On-Chip Antenna

Fig. 1 shows the geometry of the presented dual-band on-chip antenna, which is designed on an MgO substrate (relative permittivity: 9.63) with thickness of 0.5 mm. A high-resistivity silicon (Si) hemispherical lens (relative permittivity: 11.9) is attached on the back of the MgO substrate to achieve highly directional radiation in the negative Z direction. On top of the MgO is a dual-band gold thin-film antenna, where two pairs of different structured twin-slots (i.e. the longer meander and shorter straight ones) dominate the resonant radiations at the operating frequencies of 160 GHz and 640 GHz, respectively. The meander slots used for the lower frequency band is mainly for improving the symmetry of the radiation patterns in the XZ and YZ planes. In addition, a carefully designed coplanar wave-guide (CPW) network is integrated with the twin-slots to optimize the impedance matching and radiation characteristics of both frequency bands to the HTS Josephson junction, thus significantly enhancing the coupling of signal power into the junction. The CPW design also includes a fifth-order stepped-impedance choke filter to prevent the sub-THz signals from leaking onto the microwave port.

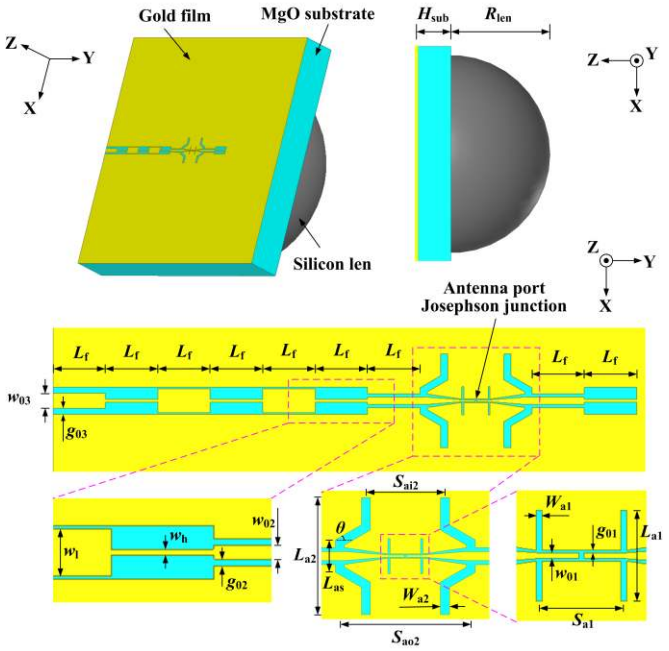


Fig. 1. Geometry of a dual-band sub-THz on-chip antenna ($H_{sub}$ = 0.5 mm, $R_{len}$ = 1.5 mm, $L_f$ = 202 $\mu$m, $L_{a1}$ = 108 $\mu$m, $W_{a1}$ = 7 $\mu$m, $S_{a1}$ = 101 $\mu$m, $L_{a2}$ = 360 $\mu$m, $L_{as}$ = 100 $\mu$m, $W_{a2}$ = 28 $\mu$m, $S_{ai2}$ = 244 $\mu$m, $S_{ao2}$ = 404 $\mu$m, $\theta$ = 30°, $w_h$ = 12 $\mu$m, $w_l$ = 92 $\mu$m, $w_{01}$ = 7 $\mu$m, $g_{01}$ = 3 $\mu$m, $w_{02}$ = 28 $\mu$m, $g_{02}$ = 12 $\mu$m, $w_{03}$ = 56 $\mu$m, $g_{03}$ = 24 $\mu$m).

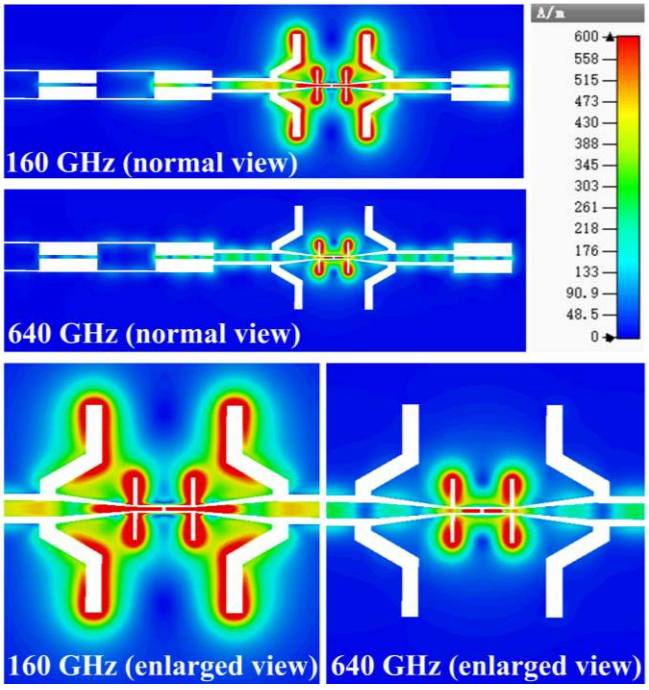


Fig. 2. Simulated surface electric current distribution on the dual-band on-chip antenna at the frequencies of 160 GHz and 640 GHz.

The antenna's design and operation principle can be explained through the surface electric current distribution (see Fig. 2), which is obtained by numerical simulations using the software Computer Simulation Technology (CST) Microwave Studio [23]. Clearly, there are electric currents surrounding both the shorter and longer twin-slots at the frequency of 160 GHz. Nevertheless, it should be pointed out that the non-resonant straight slots actually contribute very little to the

160-GHz radiation except for introducing a small inductance. The two meander slots are dominant radiators at 160 GHz, and the farthest spacing (see $S_{ao2}$ in Fig. 1) between them is approximately half guided wavelength ($\lambda_g$ / 2). Therefore, the high input impedance of the meander slots can be transformed via the $\lambda_g$ / 4 CPW sections into a much lower value at the antenna port. Due to the parasitic series inductances induced by the straight slots, the overall equivalent path lengths of the meander slots are slightly longer than $\lambda_g$ / 2. At 640 GHz, the electric currents mainly concentrate near the shorter straight twin-slots that dominate the resonant radiations. Similar to the lower frequency band, two $\lambda_g$ / 4 CPW sections between the straight slots are utilized to minimize the antenna-junction impedance mismatch. Two additional CPW sections are introduced on the right of the meander slots to achieve a virtual 'short' boundary for the straight slots. These sections do not destroy the 'short' boundary condition for the meander slots when operating at the lower frequency. Finally, as clearly seen from Fig. 2, the electric currents at 160 and 640 GHz are both effectively isolated from the intermediate-frequency (IF) microwave port at the leftmost end.

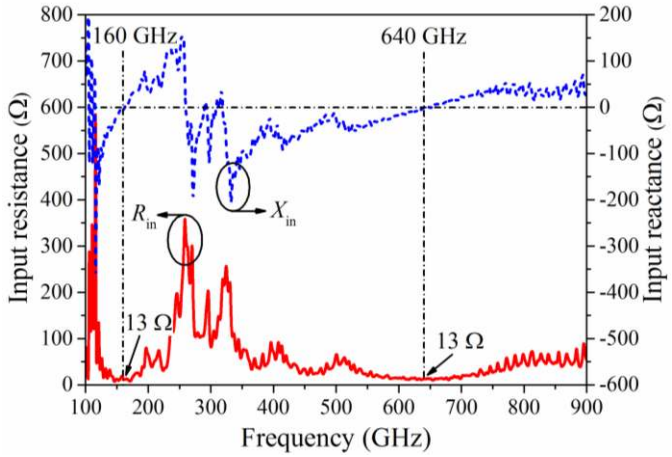


Fig. 3. Simulated input impedance of the dual-band on-chip antenna. (Red: input resistance $R_{in}$; blue: input reactance $X_{in}$.)

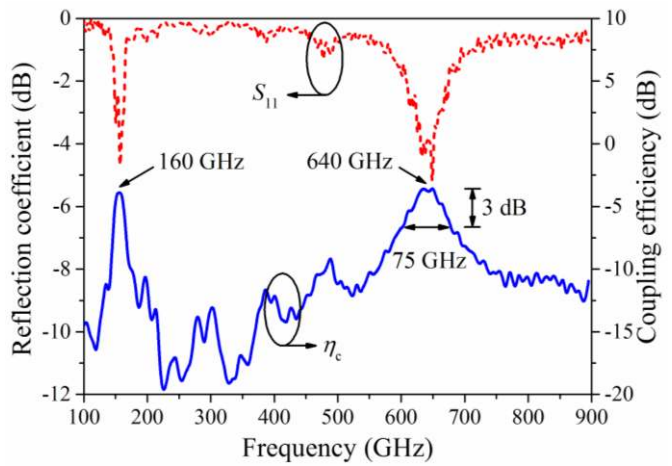


Fig. 4. Simulated reflection coefficient and coupling efficiency of the dual-band on-chip antenna. (Red: reflection coefficient $S_{11}$; blue: coupling efficiency $\eta_c$.)

Detailed simulation results of the dual-band on-chip antenna have been obtained with the CST software, including the input impedance, reflection coefficient, coupling efficiency and radiation patterns. As clearly shown in Fig. 3, the antenna resonates at the frequencies of 160 GHz and 640 GHz, and exhibits a low input resistance $R_{in}$ of around 13 Ω at both frequency bands. The small value of $R_{in}$ is close to that of the junction normal resistance $R_n$ (typically 1 to 10 Ω), thus significantly reducing the power loss due to the impedance mismatch between the antenna and Josephson junction. Fig. 4 shows that a reflection coefficient $S_{11}$ of around -4.5 dB is achieved at those two frequencies of interest, where the antenna port impedance is chosen to be the $R_n$ value (i.e. 3 Ω) as extracted from the measured junction characteristics of the HTS fourth-harmonic mixer prototype discussed in later section. A coupling efficiency $\eta_c$ is defined for the dual-band on-chip antenna to describe its capability of coupling radiations into the Josephson junction, which is denoted as

$$\eta_c = \left(1 - |S_{11}|^2\right)\eta \tag{1}$$

where $\eta$ is the radiation efficiency. As shown in Fig. 4, the antenna has a coupling efficiency of -3.7 dB at both operating frequencies, and a 3-dB available bandwidth of 20 GHz for the 160-GHz and 75 GHz for the 600-GHz frequency bands, respectively.

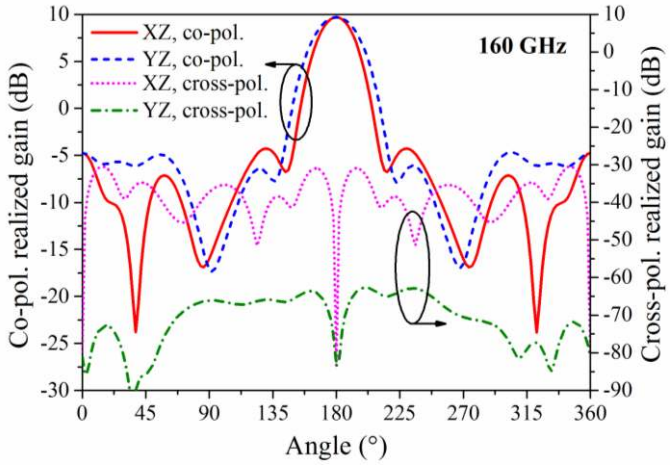


(a)

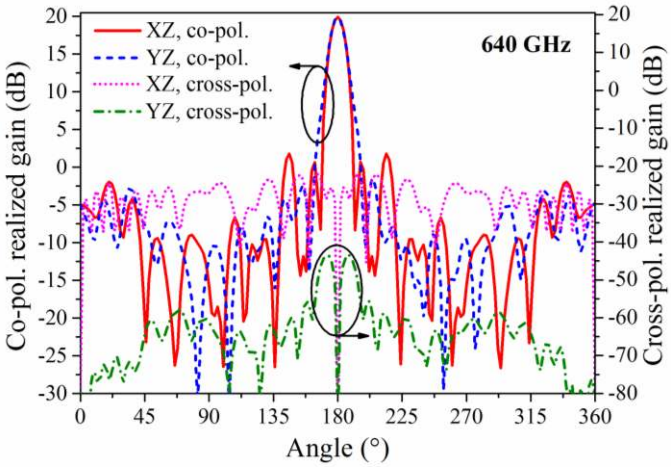


(b)

Fig. 5. Simulated radiation patterns of the dual-band on-chip antenna at (a) 160 GHz and (b) 640 GHz. (Red: co-polarization patterns in the XZ plane; blue: co-polarization patterns in the YZ plane; pink: cross-polarization patterns in the XZ plane; green: cross-polarization patterns in the YZ plane.)

Fig. 5 shows the simulated co-polarization and cross-polarization radiation patterns at the frequencies of 200 GHz and 600 GHz. Clearly, the radiation patterns exhibit high directivity towards the negative Z direction and very good symmetry in the XZ and YZ planes. As well understood from the fixed aperture size of the Si lens, the half-power beam width (HPBW) reduces from 34° at 160 GHz to 10° at 640 GHz. The co-polarization realized gains of the on-chip antenna are 9.7 dB and 19.9 dB for the lower and higher operating frequency bands, respectively. The cross-polarization levels are extremely low (less than -40 dB for both frequencies of interest), which indicates that the bent current paths of the meander slots would not deteriorate the polarization characteristics of the on-chip antenna. In addition, the side-lobe and back-lobe levels are all below -14 dB for the 160-GHz and -18 dB for the 640-GHz frequency bands, respectively.

## III. HTS Josephson-Junction Sub-THz Fourth-Harmonic Mixer

### A. Mixer Implementation and Experiment

Based on the designed dual-band on-chip antenna, a HTS Josephson-junction fourth-harmonic mixer was experimentally implemented using the CSIRO in-house developed $YBa_2Cu_3O_{7-x}$ (YBCO) step-edge junction technology [19]. Fig. 6(a) shows a micrograph of the fabricated mixer device chip, where a HTS Josephson junction is integrated at the feeding port of the dual-band thin-film antenna, and a 50-Ω tapered CPW line is utilized to the left of the choke filter to facilitate the wire bonding for DC and IF connections. The straight and meander twin-slot radiators are shown more clearly by the inset of Fig. 6(a), where a step pattern was created in-between the two straight slots by using a standard photolithography and Ar-ion beam etching techniques on the MgO substrate prior to the YBCO film deposition [19]. Fig. 6(b) shows an enlarged view of the HTS YBCO step-edge junction, that is a 2-$\mu$m wide YBCO strip across the step edge forming a grain boundary Josephson junction (the black colored section in the middle). The YBCO lines beneath the gold film connecting the junction are for DC biasing and measuring the DC current-voltage characteristics (IVCs) of the junction. To ensure a minimal contact resistance between the Au antenna and YBCO film, 50 nm in-situ Au was deposited on top of the YBCO film [24]. In subsequent processing steps, the in-situ Au was then removed everywhere except for the DC lines and contact pads for wiring bonding. A second layer of 300 nm Au was then deposited and patterned for the antenna. In this way, the contact impedance between the Au antenna and YBCO film is negligible. The HTS mixer chip was packaged using the proposed method in [16] and the packaged fourth-harmonic mixer module is shown in the inset of Fig. 7. Two identical 3-mm lens-antenna-coupled HTS mixer devices were fabricated on a 10×10-mm$^2$ MgO chip (see Fig. 7), thus reducing the fabrication cost and providing a second back-up device. In-house designed bias-tees [15] were integrated in the module to achieve good isolation between the DC and IF signals.

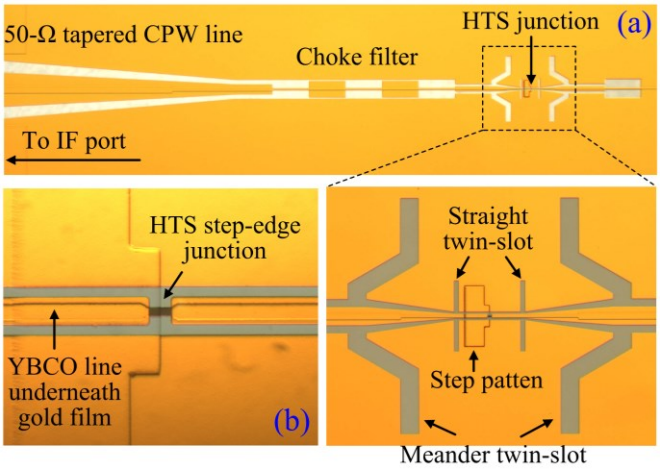


Fig. 6. (a) A micrograph of the fabricated dual-band antenna-coupled HTS mixer chip; the inset clearly shows the straight and meander twin-slots as well as the step pattern. (b) An enlarged view showing the YBCO step-edge Josephson junction and the DC biasing lines beneath the gold film.

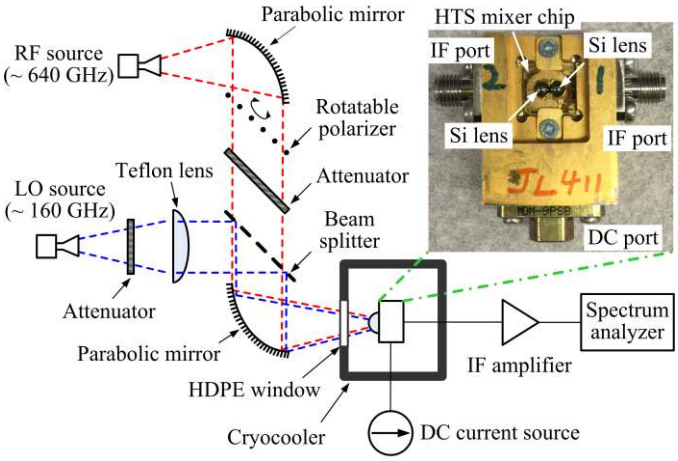


Fig. 7. The schematic diagram of fourth-harmonic mixing measurement set-up for the presented HTS mixer; the inset shows a packaged mixer module with two identical 3-mm lens-antenna-coupled HTS mixer devices fabricated on a 10×10-mm$^2$ MgO chip.

The dual-band antenna-coupled HTS mixer was measured at the frequencies near 640 GHz in a fourth-harmonic mixing mode. The schematic diagram of the mixing experimental set-up is shown in Fig. 7. The HTS mixer module was mounted in a temperature adjustable cryocooler [22] with its Si hemispherical lens facing the window. The RF (~ 640 GHz) and LO (~ 160 GHz) signals were generated by two commercial solid-state sources [Active Multiplier Chains (AMCs)] from VDI and Millitech, respectively. Those two radiation beams, after being collimated by an off-axis parabolic mirror or a Teflon plano-convex lens, were combined via a beam splitter and then coupled onto the Si lens of the mixer module. Under an appropriate DC bias provided by a battery-operated current source, heterodyne mixing occurs between the RF input signal and the fourth harmonic of the LO pumping signal. The down-converted IF output signal was amplified by a low noise amplifier (LNA) [25] with a gain of 35-40 dB from 0.3 to 16 GHz at room temperature, and then recorded using an Agilent E4407B spectrum analyzer. In addition, a quasi-optical attenuator together with a rotatable

wire-grid polarizer were included in the RF quasi-optical link to achieve a large amount of signal attenuation and a wide range of power variations for the mixer linearity characterization. Another attenuator was also utilized in the LO link to investigate the influence of LO pumping power $P_{LO}$ on the mixer performance. The different values of $P_{LO}$ were obtained by changing the attenuator with different attenuation levels.

### *B. Measurement Results*

The HTS mixer was characterized in a wide range of operating temperatures from 20 to 77 K. Fig. 8(a) shows the measured DC IV curves of the HTS Josephson junction, which displays a well-defined resistively-shunted-junction (RSJ) behavior at all measured temperatures, with a normal resistance $R_n \approx 3\ \Omega$ and a junction critical current $I_c$ between 40 $\mu$A (77 K) and 608 $\mu$A (20 K). Under the illumination of RF and LO signals, as clearly shown in Fig. 8(b), the junction IV curve changes with a strong $I_c$ suppression and a series of Shapiro steps induced at the voltages $V_n = n\Phi_0 f_{sig}$ [26] (where $n$ is an integer, $\Phi_0$ is the magnetic flux quantum, and $f_{sig}$ is the signal frequency). As predicted by the above Josephson voltage-frequency relationship, the Shapiro voltage step induced by LO pumping (~ 160 GHz) is around a quarter of that by the RF signal (~ 640 GHz). The results in Fig. 8(b) showed that both the RF and LO radiations are effectively coupled into the Josephson junction via the dual-band on-chip antenna.

Figs. 9-13 show the measured frequency down-conversion performance of the fourth-harmonic mixer. Except for linearity characterization, the mixer was always operated in its linear region by applying a suitable amount of attenuation to the RF input signal. This was achieved by using a fixed attenuator and setting the rotation angle $\alpha$ of the wire-grid polarizer to 80° (where $\alpha$ = 0° corresponds to a maximum signal transmission with no polarization mismatch). Fig. 9 illustrates the relationship of the IF output power versus bias current under different LO pumping power levels. Clearly, the measured IF output power $P_{IF}$ at 2.4 GHz (generated from fourth-harmonic mixing between $f_{RF}$ = 642.24 GHz and $f_{LO}$ = 159.96 GHz), is strongly dependent on the bias current $I_b$ with a modulation behavior. By plotting $P_{IF}$ versus $I_b$ together with the DC IV curve under LO pumping in Fig. 10, it can be seen that the IF output peaks are achieved when $I_b$ is located halfway between the adjacent Shapiro steps, where the dynamic resistance $R_D = dV / dI_b$ (the slope of the IV curve) reaches the maximum. The best $P_{IF}$ is achieved at the second IF output peak (see Fig. 10) where the $R_D$ also has the highest value (at the middle point of the 2nd Shapiro voltage step). Furthermore, as shown in Fig. 9, the IF peaks move leftward with increasing LO power $P_{LO}$; the highest value of $P_{IF}$ being relatively insensitive to the variation of $P_{LO}$. The peak shift can be well understood from more $I_c$ suppression for higher $P_{LO}$ values, thus a lower $I_b$ value is needed for the first $P_{IF}$ peak. The $P_{LO}$ (coupled into the junction) for normal operation was estimated to be around -43.7 dBm from the measured IV curve shown in Fig. 10, much lower than that required for pumping a semiconductor mixer [27].

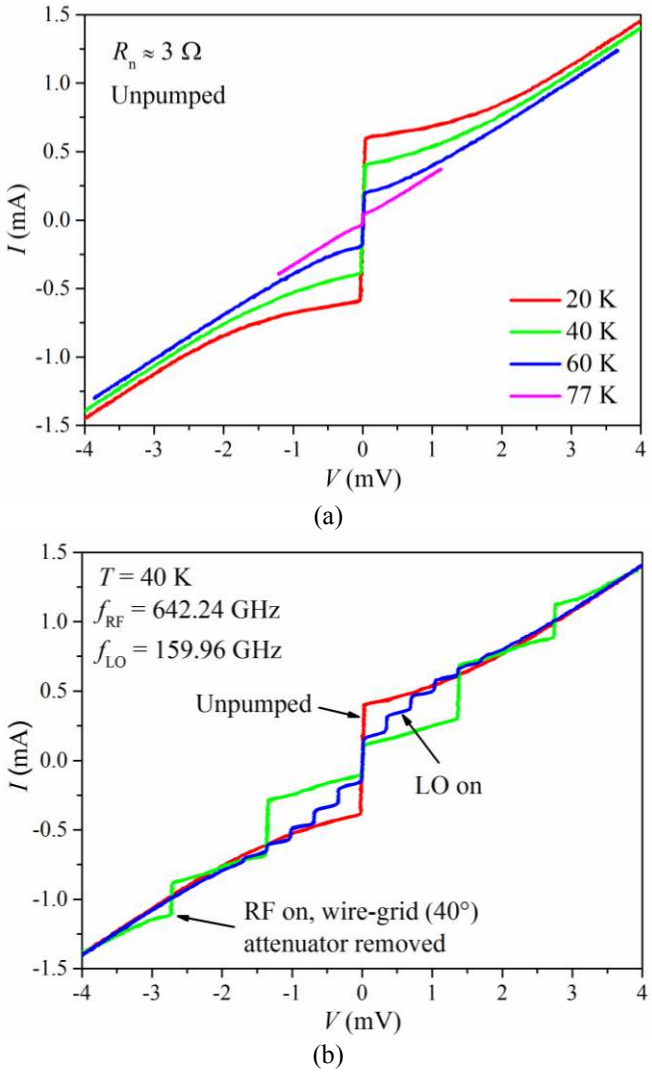


Fig. 8. DC IV curves of the HTS Josephson fourth-harmonic mixer when (a) unpumped and (b) pumped with RF and LO signals.

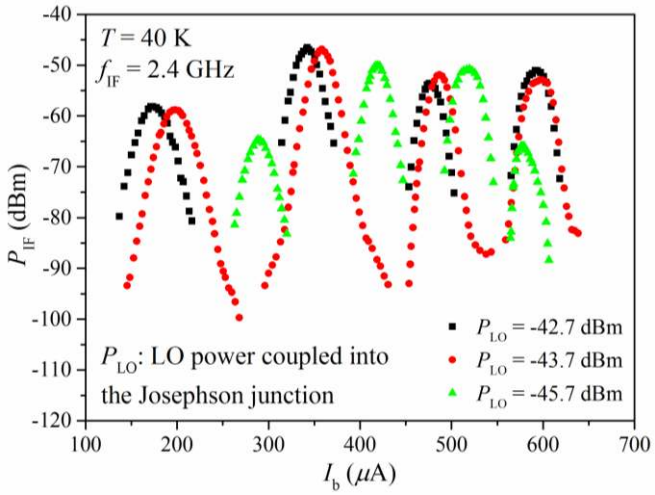


Fig. 9. IF output power $P_{IF}$ versus bias current $I_b$ for different LO pumping levels.

Fig. 11 shows the measured linearity of the mixer at the temperature of 40 K. The RF input power, $P_{RF}$, coupled into the Josephson junction, was estimated to be around -46.8 dBm at a

wire grid angle $\alpha$ = 40°. This was actually obtained by measuring the $I_c$ suppression and Shapiro current step-height on the RF pumped DC IV curve [see the green curve in Fig. 8(b)] and adding a 16.7-dB power loss (imposed by the fixed attenuator in the RF link). The values of $P_{RF}$ at other polarizer rotation angles, was obtained through an attenuation calibration for the rotatable wire-grid polarizer using a VDI detector. As shown in Fig. 11, a very good linear relationship is achieved for $P_{IF}$ and $P_{RF}$ below $P_{RF}$ ~ -50 dBm.

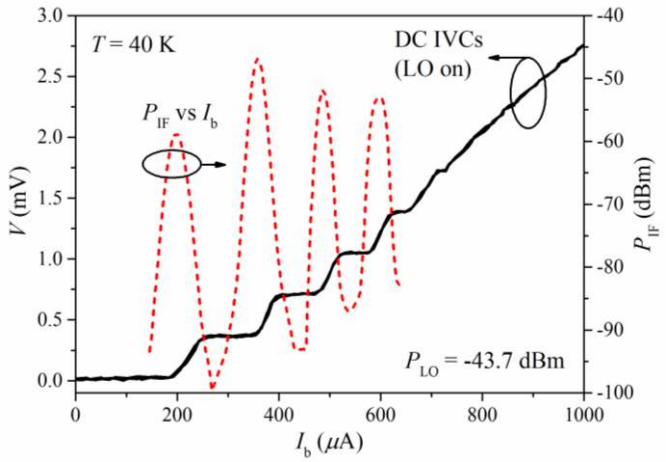


Fig. 10. IF output power $P_{IF}$ versus bias current $I_b$, plotted together with the DC IV curve under LO pumping.

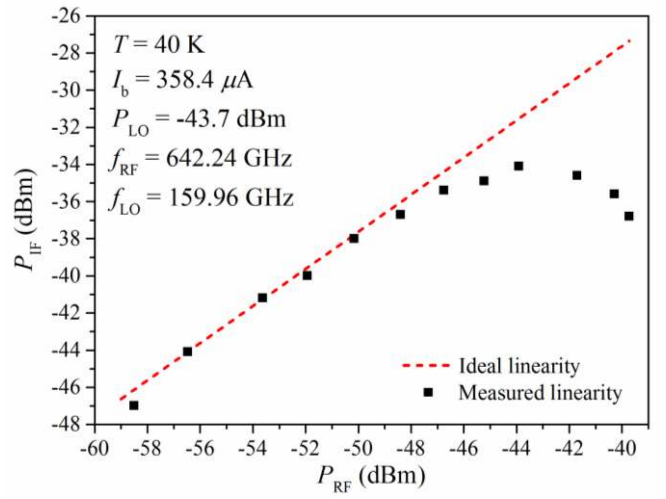


Fig. 11. Linearity of the HTS fourth-harmonic mixer.

Fig. 12 shows the characterized double-sideband (DSB) frequency response of the HTS fourth-harmonic mixer. Operating with a fixed $f_{LO}$ of 159.96 GHz and a varied $f_{RF}$ from 615.84 to 657.84 GHz, the mixer outputs a down-converted IF frequency range of 0.96 to 24 GHz in the lower sideband and 0.96 to 18 GHz in the upper sideband, respectively. The measured $P_{IF}$ versus $f_{RF}$ displays roll-offs at lower and upper frequency bands (see the black solid curve), resulting from the bandwidth restrictions of the IF amplifier and RF source. After a calibration of the entire IF link (including cables and IF LNA) and the RF input power variation with operating frequency, the result is shown in Fig. 12 (the red dashed line). The mixer exhibits a very wide IF bandwidth of at least 23 GHz over the 640-GHz frequency band. To the best of our knowledge, this is the largest demonstrated IF bandwidth for HTS Josephson mixers reported to date. Such wide IF bandwidth is attributed to the following factors: (1) good on-chip antenna and circuit designs (e.g. 37.5 GHz coupling bandwidth for each sideband of 640 GHz, as shown in Fig. 4); (2) lower HTS Josephson junction capacitance, compared to that of SIS mixers, enabling wideband impedance matching; and (3) shorter response time of HTS Josephson-junction devices than that of HEB mixers restricted by relatively slow hot electron relaxation. The slight fluctuation in the frequency response traces are believed to result from the imperfect quasi-optical link as well as the measurement and calibration tolerances.

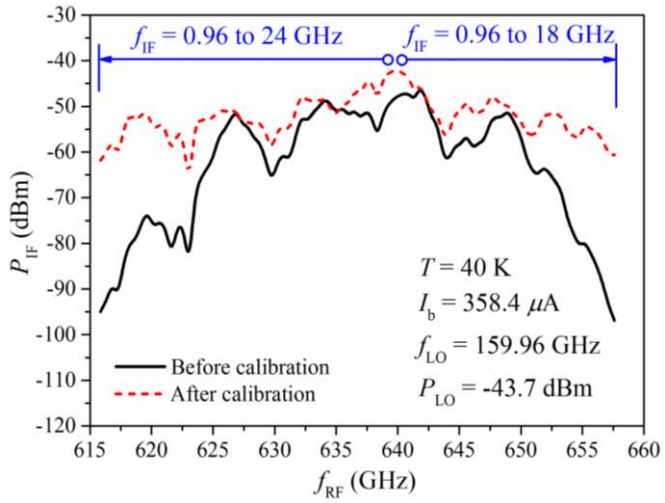


Fig. 12. DSB frequency response of the HTS fourth-harmonic mixer.

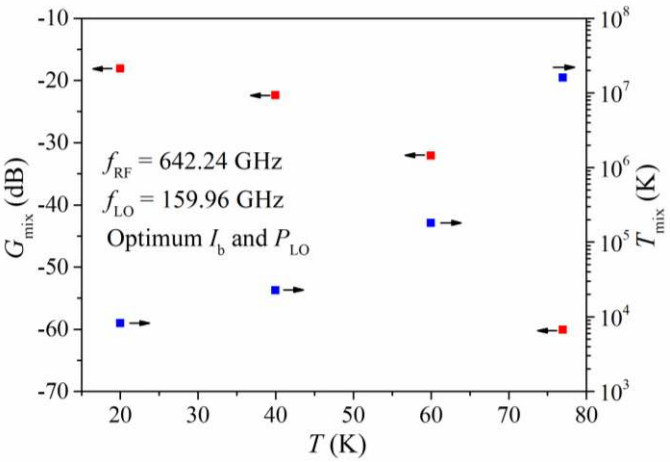


Fig. 13. Conversion gain and DSB noise temperature of the HTS fourth-harmonic mixer as well as their dependence on operating temperature.

Fig. 13 shows the measured conversion gain $G_{mix}$ of the HTS fourth-harmonic mixer and its dependence on the operating temperature $T$. The mixer gain was estimated from $G_{mix} = P_{IF} / (P_{RF} \cdot G_{IF})$ at optimum $I_b$ and $P_{LO}$ conditions, where $G_{IF}$ is the calibrated IF link gain using a vector network analyzer (VNA). As clearly shown in Fig. 13, the mixer exhibits a conversion

TABLE I. Performance comparison of state-of-the-art harmonic mixers at similar operating frequencies

| References | Device technology | Harmonic order | Operating frequency ($f_{RF}$) | Conversion loss ($1/G_{mix}$) | LO power ($P_{LO}$) | IF frequency range ($f_{IF}$) |
|---|---|---|---|---|---|---|
| [28] | LTS | 9 | 604 GHz | 55.4 dB @ 4.2K | - | ~ 1 GHz |
| [28] | LTS | 5 | 693 GHz | 43.5 dB @ 4.2K | - | ~ 1 GHz |
| [29] | Semiconductor | 4 | 325-500 GHz | 15-22 dB @ RT | 7-25 mW | - |
| [30] | Semiconductor | 4 | 600 GHz | 27 dB @ RT | 2.2 mW | 0.87 GHz |
| [15] | HTS | 20 | 614 GHz | 49 dB @ 40K | 5.6 $\mu$W | 1-3 GHz |
| [16] | HTS | 20 | 600 GHz | 50 dB @ 40K | 0.8 $\mu$W | 1-12 GHz |
| **This work** | **HTS** | **4** | **640 GHz** | **18 dB @ 20K; 22 dB @ 40K** | **50 nW** | **0.96-24 GHz** |

gain as high as -18.1 dB at 20 K and -22.4 dB at 40 K, respectively, which are the best reported results for HTS harmonic mixers to date. Furthermore, the mixer operates stably in a wide temperature range from 20 to 77 K (liquid nitrogen temperature), although $G_{mix}$ decreases with the increase of $T$ due to the decreased $R_D$ and $I_c$ at higher temperatures. Based on the measured conversion gain, the DSB mixer noise temperature, $T_{mix}$, can be estimated if the device output noise $T_{out}$ is known. With reference to [31] and [32], the $T_{out}$ of our presented mixer is obtained by numerical simulation using the following formula

$$T_{out} = \beta^2 C_{if} T R_D / R_n \quad (2)$$

where $\beta > 1$ is a dimensionless excess noise parameter, $T$ is the operating temperature, and $R_D$ and $R_n$ are the junction dynamic and normal resistances, respectively. The only difference of this formula from Eq. (6) in [31] is that, there exists a factor $C_{if}$ [32] that accounts for the coupling efficiency from the mixer output to a 50-Ω IF load. Finally, the DSB noise temperature $T_{mix} = T_{out} / (2 \bullet G_{mix})$ is obtained and shown in Fig. 13. The $T_{mix}$ value rises monotonically with the increase of $T$, about 8000 K and 22000 K at the operating temperature of 20 K and 40 K, respectively.

The results show that an excellent device performance is achieved for our dual-band antenna-coupled HTS fourth-harmonic mixer. Table I compares the performance of the presented device with other state-of-the-art harmonic mixers (based on the semiconductor, LTS and HTS technologies) at similar operating frequencies. It clearly shows that our mixer exhibits a superior performance in terms of relatively high conversion gain, low LO power, and wide IF bandwidth.

## IV. Conclusion

A dual-band on-chip antenna coupled 640-GHz HTS fourth-harmonic mixer was presented in this paper. The antenna integrates different structured twin-slots with a well-designed CPW network to achieve high-efficiency power coupling at two frequency bands. Based on the designed antenna, HTS step-edge Josephson-junction mixer was developed and characterized operating in the fourth-harmonic mixing mode. Detailed measurement results were provided, including DC characteristics, optimum biasing, LO power influence, mixing linearity, frequency response, as well as conversion gain and its temperature dependence. The measured conversion gain is around -18 dB at 20 K and -22 dB at 40 K, and the IF bandwidth at least 23 GHz over the 640-GHz operating frequency band. The required LO power is only around -43 dBm (or 50 nW), much lower than that of the semiconductor mixers. These are the best reported results for HTS sub-THz harmonic mixers to date. Compared to conventional HTS fundamental and high-order harmonic mixers, the presented concept of mixer offers a good compromise between performance and cost, thus will find huge potential in the sub-THz wireless communication and sensing applications.

## Acknowledgement

The authors would like to thank our colleagues Ms Jeina Lazar for the HTS chip fabrication and Ms Mei Shen for the mixer module packaging.

## References

[1] G. Ducournau, P. Szriftgiser, A. Beck, D. Bacquet, F. Pavanello, E. Peytavit, M. Zaknoune, T. Akalin, and J.-F. Lampin, "Ultrawide-Bandwidth Single-Channel 0.4-THz Wireless Link Combining Broadband Quasi-Optic Photomixer and Coherent Detection," *IEEE Trans. THz Sci. Technol.*, vol. 4, no. 3, pp. 328-337, May 2014. DOI: 10.1109/TTHZ.2014.2309006.

[2] T. Schneider, "Ultrahigh-bitrate wireless data communications via THz-links; possibilities and challenges," *J. Infrared Millimeter THz Waves*., vol. 36, no. 2, pp. 159-179, Feb. 2015. DOI: 10.1007/s10762-014-0100-1.

[3] D. Jasteh, E. G. Hoare, M. Cherniakov, and M. Gashinova, "Experimental low-terahertz radar image analysis for automotive terrain sensing," *IEEE Geosci. Remote Sens. Lett.*, vol. 13, no. 4, pp. 490-494, Apr. 2016. DOI: 10.1109/LGRS.2016.2518579.

[4] X. Tong, Q. Li, N. An, W. Wang, X. Deng, L. Zhang, H. Liu, J. Zeng, Z. Li, H. Tang, and Y. Xiong, "The study of 0.34 THz monolithically integrated fourth subharmonic mixer using planar schottky barrier

diode," *J. Infrared Millimeter THz Waves*., vol. 36, no. 11, pp. 1112-1122, Nov. 2015. DOI: 10.1007/s10762-015-0208-y.
[5] K. M. K. H. Leong, X. Mei, W. H. Yoshida, A. Zamora, J. G. Padilla, B. S. Gorospe, K. Nguyen, and W. R. Deal, "850 GHz receiver and transmitter front-ends using InP HEMT," *IEEE Trans. THz Sci. Technol.*, vol. 7, no. 4, pp. 466-475, Jul. 2017. DOI: 10.1109/TTHZ.2017.2710632.
[6] B. Khamaisi and E. Socher, "130-320-GHz CMOS harmonic down-converters around and above the cutoff frequency," *IEEE Trans. Microw. Theory Techn.*, vol. 63, no. 7, pp. 2275-2288, Jul. 2015. DOI: 10.1109/TMTT.2015.2431671.
[7] J. Al-Eryani, H. Knapp, J. Kammerer, K. Aufinger, H. Li, and L. Maurer, "Fully integrated single-chip 305-375-GHz transceiver with on-chip antennas in SiGe BiCMOS," *IEEE Trans. THz Sci. Technol.*, vol. 8, no. 3, pp. 329-339, May 2018. DOI: 10.1109/TTHZ.2018.2823202.
[8] J. Chen, M. Liang, L. Kang, B. B. Jin, W. W. Xu, P. H. Wu, W. Zhang, L. Jiang, N. Li, and S. C. Shi, "Low noise receivers at 1.6 THz and 2.5 THz based on Niobium Nitride hot electron bolometer mixers," *IEEE Trans. Appl. Supercond.*, vol. 19, no. 3, pp. 278-281, Jun. 2009. DOI: 10.1109/TASC.2009.2017910.
[9] T. Kojima, M. Kroug, M. Takeda, W. Shan, Y. Fujii, Y. Uzawa, Z. Wang, and S. Shi, "Performance of terahertz waveguide SIS mixers employing epitaxial NbN films and Nb junctions," *IEEE Trans. Appl. Supercond.*, vol. 19, no. 3, pp. 405-408, Jun. 2009. DOI: 10.1109/TASC.2009.2018232.
[10] J. Chen, H. Myoren, K. Nakajima, T. Yamashita, and P. H. Wu, "Mixing at terahertz frequency band using $YBa_2Cu_3O_{7-\delta}$ bicrystal Josephson junctions," *Appl. Phys. Lett.,* vol. 71, no. 5, pp. 707-709, Aug. 1997. DOI: 10.1063/1.119836.
[11] H. Shimakage, Y. Uzawa, M. Tonouchi, and Z. Wang, "Noise temperature measurement of YBCO Josephson mixers in millimetre and submillimeter waves," *IEEE Trans. Appl. Supercond.*, vol. 7, no. 2, pp. 2595-2598, Jun. 1997. DOI: 10.1109/77.621770.
[12] O. Harnack, M. Darula, J. Scherbel, J.-K. Heinsohn, M. Siegel, D. Diehl, and P. Zimmermann, "Optimization of a 115 GHz waveguide mixer based on an HTS Josephson junction," *Supercond. Sci. Technol.*, vol. 12, no. 11, pp. 847-849, Nov. 1999. DOI: 10.1088/0953-2048/12/11/346.
[13] J. Scherbel, M. Darula, O. Harnack, and M. Siegel, "Noise properties of HTS Josephson mixers at 345 GHz and operating temperatures at 20 K," *IEEE Trans. Appl. Supercond.*, vol. 12, no. 2, pp. 1828-1831, Jun. 2002. DOI: 10.1109/TASC.2002.1020345.
[14] M. Malnou, C. Feuillet-Palma, C. Ulysse, G. Faini, P. Febvre, M. Sirena, L. Olanier, J. Lesueur, and N. Bergeal, "High-Tc superconducting Josephson mixers for terahertz heterodyne detection," *J. Appl. Phys.*, vol. 116, no. 7, pp. 074505 - 074505-11, Aug. 2014. DOI: 10.1063/1.4892940.
[15] J. Du, A. R. Weily, X. Gao, T. Zhang, C. P. Foley, and Y. J. Guo, "HTS step-edge Josephson junction terahertz harmonic mixer," *Supercond. Sci. Technol.,* vol. 30, no. 2, pp. 024002, Nov. 2016. DOI: 10.1088/0953-2048/30/2/024002.
[16] X. Gao, T. Zhang, J. Du, A. R. Weily, Y. J. Guo, and C. P. Foley, "A wideband terahertz high-$T_c$ superconducting Josephson-junction mixer: electromagnetic design, analysis and characterization," *Supercond. Sci. Technol.,* vol. 30, no. 9, pp. 095011, Aug. 2017. DOI: 10.1088/1361-6668/aa7cc1.
[17] X. Gao, J. Du, T. Zhang, and Y. J. Guo, "Noise and conversion performance of a high-$T_c$ superconducting Josephson junction mixer at 0.6 THz," *Appl. Phys. Lett.,* vol. 111, no. 19, pp. 192603, Nov. 2017. DOI: 10.1063/1.5004733.
[18] J. Du, C. Pegrum, X. Gao, A. R. Weily, T. Zhang, Y. J. Guo, and C. P. Foley, "Harmonic mixing using a HTS step-edge Josephson junction at 0.6 THz frequency," *IEEE Trans. Appl. Supercond.*, vol. 27, no. 4, pp. 1500905, Jun. 2017. DOI: 10.1109/TASC.2016.2636081.
[19] C. P. Foley, E. E. Mitchell, S. K. H. Lam, B. Sankrithyan, Y. M. Wilson, D. L. Tilbrook, and S. J. Morris, "Fabrication and characterisation of YBCO single grain boundary step edge junctions," *IEEE Trans. Appl. Supercond.*, vol. 9, no. 2, pp. 4281-4284, Jun. 1999. DOI: 10.1109/77.783971.
[20] C. A. Balanis, *Antenna Theory: Analysis and Design*. New York, USA: Wiley, 1992.
[21] P. Focardi, W. R. McGrath, and A. Neto, "Design guidelines for terahertz mixers and detectors," *IEEE Trans. Microw. Theory Tech.*, vol. 53, no. 5, pp. 1653-1661, May 2005. DOI: 10.1109/TMTT.2005.847058.
[22] J. Du, J. C. Macfarlane, S. H. K. Lam, and R. T. Taylor, "HTS Josephson heterodyne oscillator on a pulse-tube cryocooler," *Supercond. Sci. Technol.*, vol. 22, no. 10, pp. 105013, Sep. 2009. DOI: 10.1088/0953-2048/22/10/105013.
[23] CST, [online] Available: http://www.cst.com.
[24] J. Du, S. K. H. Lam, and D. L. Tilbrook, "Metallization and interconnection of HTS YBCO thin film devices and circuits," *Supercond. Sci. Technol.*, vol. 14, no. 10, pp. 820-825, Sep. 2001. DOI: 10.1088/0953-2048/14/10/303.
[25] LNF-LNC0.3_14A, [online] Available: http://www.lownoisefactory.com.
[26] T. V. Duzer and C. W. Turner, *Principles of Superconductive Devices and Circuits*. Upper Saddle River, NJ, USA: Prentice-Hall, 1999.
[27] Mixers, [online] Available: http://www.vadiodes.com.
[28] M. Kobayashi, S. Ohara, A. Katsuno, K. Sakai, and Y. Hayashi, "Harmonic mixing with SIS tunnel junctions in the millimeter and submillimeter regions," *Jpn. J. Appl. Phys.*, vol. 24, no. 12, pp. 1623-1626, Dec. 1985. DOI: 10.1143/JJAP. 24.1623.
[29] J. Deng, Q. Lu, D. Jia, Y. Yang, and Z. Zhu, "Wideband fourth-harmonic mixer operated at 325-500 GHz," *IEEE Microw. Wireless Compon. Lett.*, vol. 28, no. 3, pp. 242-244, Mar. 2018. DOI: 10.1109/LMWC.2018.2804158.
[30] J. Schur, M. Ruf, and L. P. Schmidt, "A 4th harmonic Schottky diode mixer-facilitated access to THz frequencies," *in Proc. 33rd Int. Conf. Infr., Millim. THz Waves*, Sep. 2008, pp. 1-2.
[31] J. H. Claassen and P. L. Richards, "Performance limits of a Josephson-junction mixer," *J. Appl. Phys.*, vol. 49, no. 7, pp. 4117-4129, Jul. 1978. DOI: 10.1063/1.325374.
[32] Y. Taur, "Characteristics of a Josephson junction harmonic mixer with external pumping," IEEE Trans. Magn., vol. 15, no. 1, pp. 465-467, Jan. 1979. DOI: 10.1109/TMAG.1979.1060114.

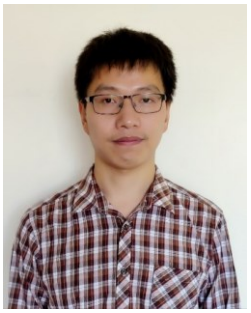

**Xiang Gao** was born in Jiangsu, China, in 1985. He received a Bachelor Degree from Nanjing University of Posts and Telecommunications, Nanjing, China, in 2006, a Master Degree from Beijing Jiaotong University, Beijing, China, in 2009, and a Ph.D. degree from Graduate University of Chinese Academy of Sciences, Beijing, China, in 2012, all in Electronic Engineering.

From 2012 to 2014, he was an Assistant Professor with Institute of Electronics, Chinese Academy of Sciences (IECAS), Beijing, China. From 2014 to 2015, he was a Research Fellow with Nanyang Technological University (NTU), Singapore. From 2015 to 2018, he worked as an Office of the Chief Executive (OCE) Postdoctoral Fellow with the Commonwealth Scientific and Industrial Research Organisation (CSIRO), Australia. Since August 2018, he has been a CSIRO Research Scientist. His research interests include antennas, superconducting devices, and terahertz imaging and communication technologies.

**Jia Du** received her B.S. from Xidian University, China, in 1982, M.S. from University of Electronic Science and Technology of China in 1984, and Ph.D. from the University of Technology, Sydney, Australia, in 1993. She was a Postdoctoral Research Fellow at National Inst of Materials and Chemical Research, Japan in 1993-1994. She joined CSIRO in 1995 and is currently a Senior Principal Research Scientist and Leader of Superconductivity Research Team. She is an Adjunct Professor at University of Technology, Sydney, since 2015.

She has extensive research experience in a broad range of interdisciplinary areas of electronic materials, devices and applied systems including semiconductor and superconductor materials and devices, composite materials, surface acoustic biosensor. In recent years, she has pioneered and led the major capability development of high-$T_c$ superconducting (HTS) Josephson junctions, SQUIDs, other novel devices and systems for terahertz imaging and wireless communication applications. She has published 88 refereed papers in

international journals, over 100 conference proceeding papers, with 1570 citations. She has served as editor, lead editor and editor-in-chief for IEEE TAS special issues and various international conference committees. She chaired International workshop on superconducting sensors and detectors - IWSSD 2018.

**Ting Zhang** received his Bachelor Degree in electronics engineering and information science from University of Science and Technology of China (UTSC), China, in 2007, and a Ph.D. Degree in Microelectronics and solid-state electronics from University of Chinese Academy of Science in 2013.

From 2013 to 2016, he was a Postdoctoral Research Fellow with the Commonwealth Scientific and Industrial Research Organisation (CSIRO), Australia. Since 2017, he has been a Chancellor's Postdoctoral Research Fellow with the Global Big Data Technology Center (GBDTC), University of Technology Sydney (UTS), Australia.

**Y. Jay Guo** (Fellow'2014) received a Bachelor Degree and a Master Degree from Xidian University in 1982 and 1984, respectively, and a PhD Degree from Xian Jiaotong University in 1987, all in China. His research interest includes antennas, mm-wave and THz communications and sensing systems as well as big data technologies. He has published over 400 research papers and holds 24 patents in antennas and wireless systems. He is a Fellow of the Australian Academy of Engineering and Technology, a Fellow of IEEE and a Fellow of IET, and a member of the College of Experts of Australian Research Council (ARC). He has won a number of most prestigious Australian national awards, and was named one of the most influential engineers in Australia in 2014 and 2015.

Prof Guo is a Distinguished Professor and the founding Director of Global Big Data Technologies Centre at the University of Technology Sydney (UTS), Australia. Prior to this appointment in 2014, he served as a Director in CSIRO for over nine years, directing a number of ICT research portfolios. Before joining CSIRO, he held various senior technology leadership positions in Fujitsu, Siemens and NEC in the U.K.

Prof Guo has chaired numerous international conferences. He was the International Advisory Committee Chair of IEEE VTC2017, General Chair of ISAP2015, iWAT2014 and WPMC'2014, and TPC Chair of 2010 IEEE WCNC, and 2012 and 2007 IEEE ISCIT. He served as Guest Editor of special issues on "*Antennas for Satellite Communications*" and "*Antennas and Propagation Aspects of 60-90GHz Wireless Communications*," both in IEEE Transactions on Antennas and Propagation, Special Issue on "*Communications Challenges and Dynamics for Unmanned Autonomous Vehicles*," IEEE Journal on Selected Areas in Communications (JSAC), and Special Issue on "*5G for Mission Critical Machine Communications*", IEEE Network Magazine.